Supporting information: Exchange Coupling Inversion in a High-Spin Organic Triradical Molecule

R. Gaudenzi,[†] E. Burzurí,[*,†] D. Reta,[‡] I. de P. R. Moreira,[‡] S. T. Bromley,[‡] C. Rovira,[¶] J .Veciana,[¶] and H. S. J. van der Zant[†]

Kavli Institute of Nanoscience, Delft University of Technology, 2600 GA, Delft, The Netherlands, Departament de Química Física and Institut de Química Teórica i Computacional, Universitat de Barcelona (IQTCUB), E-08028 Barcelona, Spain, and Institut de Ciéncia de Materials de Barcelona (ICMAB-CSIC) and CIBER-BBN, Campus de la UAB, 08193, Bellaterra, Spain

E-mail: e.burzurilinares@tudelft.nl

In this supporting information we provide experimental and theoretical details on transport and orbital characteristics of the all-organic triradical molecule subject of our study. Section 1 contains details on the molecule, junction preparation and experimental procedure. Section 2 is dedicated to gate-dependent measurements related to samples A and B and to an overview of the additional samples. Section 3 contains additional information on the calculations and the investigated potential energy surface. The dihedral angle θ is also illustrated with a graphical aid.

*To whom correspondence should be addressed

†Kavli Institute of Nanoscience, Delft University of Technology, 2600 GA, Delft, The Netherlands

‡Departament de Química Física and Institut de Química Teórica i Computacional, Universitat de Barcelona (IQTCUB), E-08028 Barcelona, Spain

¶Institut de Ciéncia de Materials de Barcelona (ICMAB-CSIC) and CIBER-BBN, Campus de la UAB, 08193, Bellaterra, Spain

1. Methods

Molecule

The studied molecule is the diasteromeric form with a C_2 symmetry of 2,4,6-trichloro-α,α,α',α',α'',α''-hexakis(pentachlorophenyl)mesityltriyl radical, prepared as previously reported.[1]

Junction preparation

The molecular solution is prepared in a water-free glove-box dissolving the molecular powder in nitrogen-saturated dichlorobenzene solvent to reach a concentration of about 0.5 mM. The molecular solution is then drop-casted onto a Si/SiO2 chip containing an array of 24 Au bridges 100-nm wide, 400 nm long and 12 nm thick with an Al/Al2O3 local gate underneath. A nano-gap is produced by feedback-controlled electromigration[2] of each of these bridges. As the bridge conductance reaches 3-4 G_0, electromigration is stopped and the wire is let self-break at room temperature. The molecular solution is evaporated while evacuating the chamber and the sample is cooled down. In the present study, six so-formed molecular junctions are investigated.

Experiment

Measurements are performed in high vacuum ($p < 5 \cdot 10^{-4}$ mbar) in a dilution refrigerator ($\approx$ 70 mK) equipped with a superconducting magnet allowing magnetic fields up to 9 T. Current spectra are extracted applying a DC bias voltage V to the gold electrodes while recording current I. The differential conductance $\mathrm{d}I/\mathrm{d}V$ is then obtained by taking the numerical derivative.

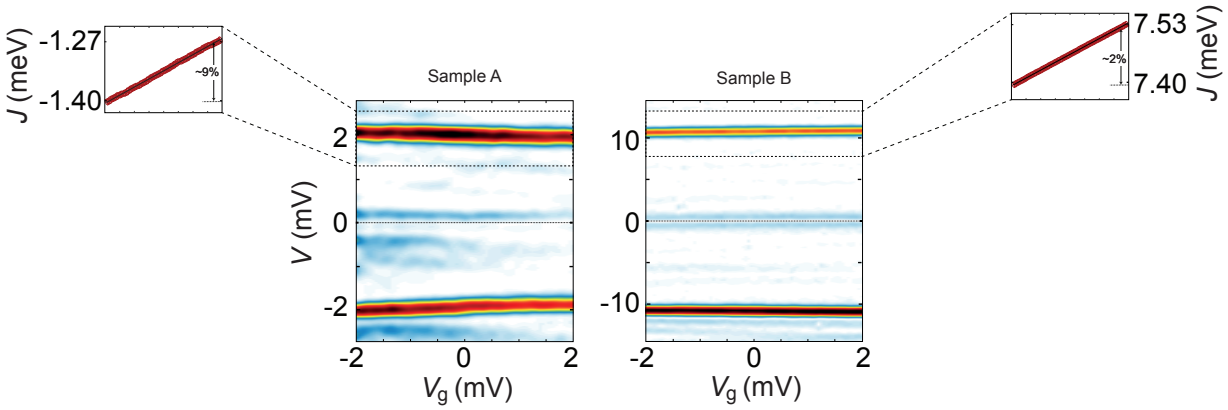

Figure S1: **Off-resonant transport and electric tunability of the exchange coupling.** $|\mathrm{d}^2I/\mathrm{d}V^2|$ color maps as a function of gate and bias voltage for samples A (left) and B (right). In the whole accessible gate range, no signs of resonant transport are visible. A fit of the peak positions reveals a tunability of J-value with applied electrostatic field. Modulations amount to 9% and 2% for A and B respectively. In both cases J increases in going from negative to positive gate voltages.

2. Off-resonant transport, electric tunability of the exchange coupling and overview of the additional samples

Gate measurements

In Figure S1 we show the $|\mathrm{d}^2I/\mathrm{d}V^2|$ color maps as a function of gate voltage V_g for samples A and B. These maps are taken sitting at $B = 0$ T in the maps of Fig. 2(c) and Fig. 3(c) and changing the gate voltage. The off-resonant character of transport is left unchanged by the gate voltage and does not exhibit any proximity to a charge degeneracy point. This is consistent with the large calculated SOMO-SUMO gap and supports charge neutrality. Noteworthy is the monotonical variation induced by the gate on the energy of the excitation: from -2.1 meV to -1.9 meV for sample A and from 11.1 V to -11.3 V for sample B in going from at $V_\mathrm{g} = -2$ V to $+2$ V. The J-values are extracted by fitting the peak and translating the energy into the corresponding exchange coupling. We quantify the electric field-induced increase of J to be 9% and 2% for samples A and B respectively, thus showing a modest electrical control of the magnetic parameters.

Table S1: Table of J-values and zero-field splittings (ZFS) relative to the measured samples. Samples exhibiting ferromagnetic and antiferromagnetic exchange couplings are grouped in the first and second block respectively. The last column indicates whether any sign of resonant transport is visible in the gate-dependent measurements.

SAMPLE	J (meV)	ZFS (meV)	Resonant transport
A	- 1.3 ± 0.1	0.15 ± 0.1	No
D	- 2.2 ± 0.1	0.15 ± 0.1	No
E	- 2.3 ± 0.4	0.05 ± 0.05	No
B	+ 7.5 ± 0.1	< 0.4	No
C	+ 0.4 ± 0.1	< 0.2	No
F	+ 2.6 ± 0.1	-	No

Statistics and Additional samples

In this study we have electromigrated and measured 120 junctions, none of which showed signs of resonant transport as expected from the energy level scheme of Fig. 5(a). For this reason, the presence of inelastic cotunneling is considered as the signature of the formation of a molecular junction. According to this criterion, 6 junctions were selected as containing the molecule. A summary of the main features of each of the six selected samples is given in Table S1.

In Fig.S2 we show the $\mathrm{d}I/\mathrm{d}V$ and $|\mathrm{d}^2I/\mathrm{d}V^2|$ color maps relative to the additional samples D and E. The presence of low- and high-bias steps shifting parallel to each other as the magnetic field is increased follows from the $S = 3/2$ high-spin ground state and $S = 1/2$ excited multiplet. This behaviour is analogous to the one observed in sample A and signals a ferromagnetic (negative) J-value. In Fig.S3 $\mathrm{d}I/\mathrm{d}V$ and $|\mathrm{d}^2I/\mathrm{d}V^2|$ color maps relative to sample F are displayed. The high-bias step split in three smaller steps at sufficiently high-magnetic fields and the low-bias step split in two steps. This behaviour results from a $S = 1/2$ low-spin ground state and a $S = 3/2$ high-spin ground state. In this case, the exchange interaction is antiferromagnetic (positive J-value) as in samples B and C of the main text.

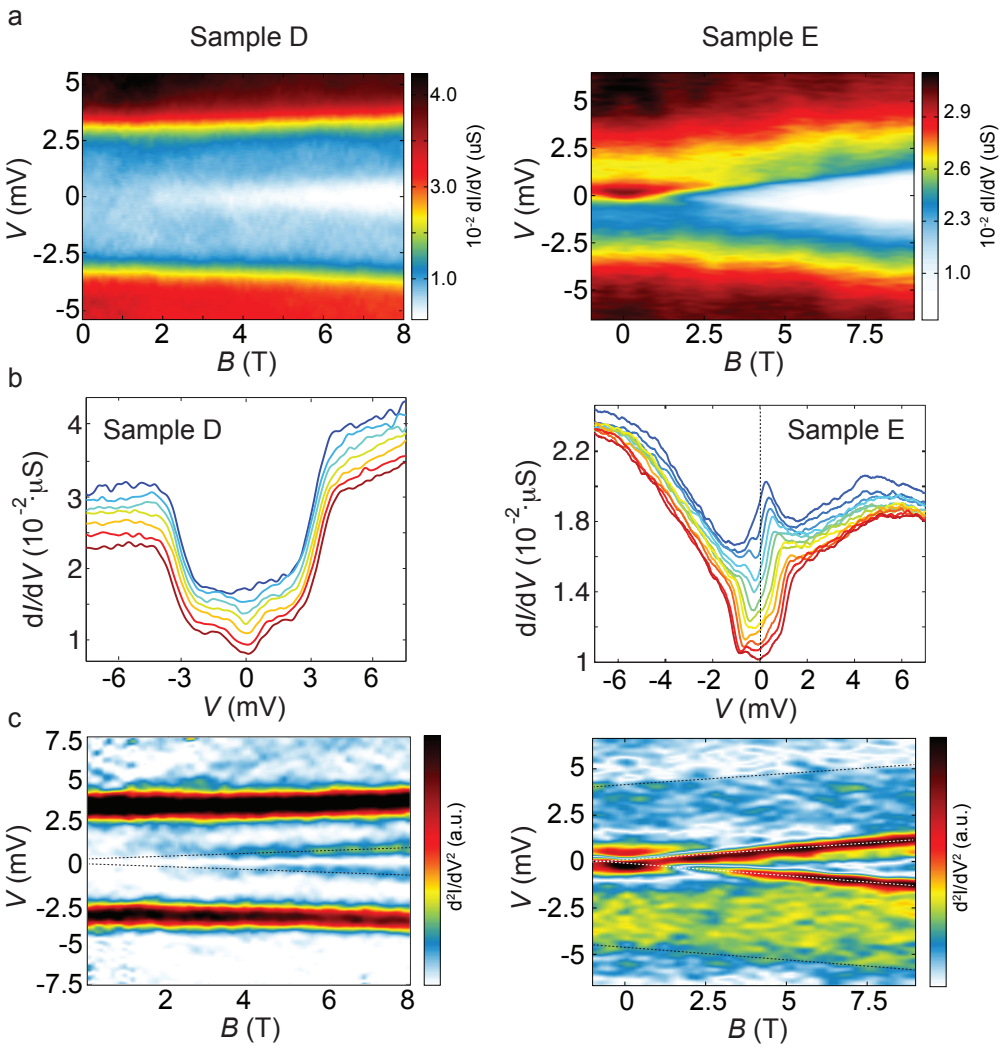

Figure S2: **Magnetic behaviour of additional samples D and E.** (a) $\mathrm{d}I/\mathrm{d}V$ color maps of samples D and E. In both samples, two steps in differential conductance shift linearly and parallel to each other in magnetic field. (b) $\mathrm{d}I/\mathrm{d}V$ linecuts extracted from the color maps in (a). (c) Corresponding $|\mathrm{d}^2I/\mathrm{d}V^2|$ color maps. This behaviour signals a high-spin ground state and is analogous to the one observed in sample A (ferromagnetic interaction), shown in the main text.

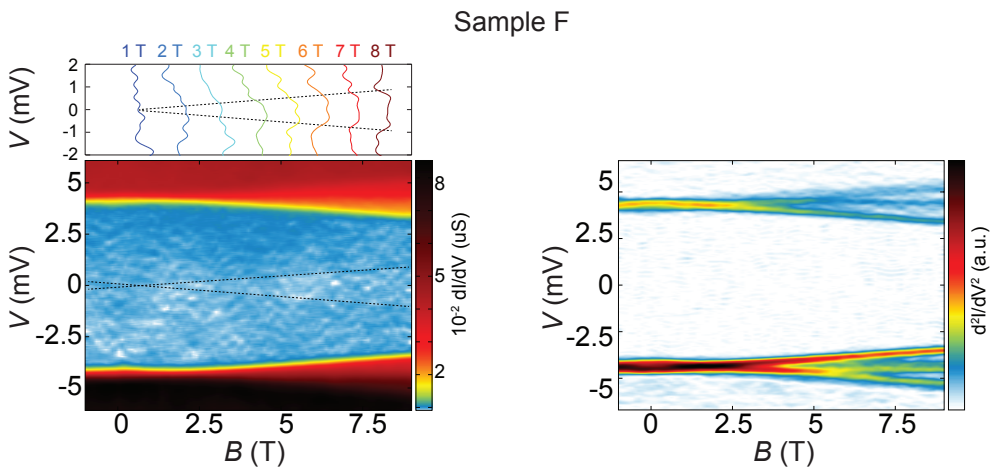

Figure S3: **Magnetic behaviour of additional sample F.** (below) $\mathrm{d}I/\mathrm{d}V$ and $|\mathrm{d}^2I/\mathrm{d}V^2|$ color maps (below) relative to sample F. Here the high-energy transition is seen splitting in three smaller steps, signalling a low-spin ground state. The transition $S_z = -1/2 \rightarrow 1/2$ within the ground state multiplet is very faintly visible and has been marked by the dashed line. (above) Linecuts extracted from the $\mathrm{d}I/\mathrm{d}V$ color map at the magnetic fields. This behaviour is analogous to that observed for sample B and C (antiferromagnetic interaction) in the main text.

3. Theoretical analysis: energy levels and isosurface, dihedral angle

Computational details

All calculations in this work were performed within the spin unrestricted density functional formalism using the Gaussian-09 suite of programs.[3] The functional used was the popular B3LYP hybrid density functional and for all atoms, the basis set employed is the standard all electron 6-31G[4–6] . Within the broken symmetry (BS) approach,[7–9] - one describes the low S_z pure spin solution (in this case a doublet state) by means of a monodeterminant solution. In order to extract the exchange coupling constant from the broken symmetry solutions, we follow the mapping approach,[10] which is further explained in the next section. The strategy followed for the extraction of the exchange coupling constant along the potential energy surface investigated consists in optimizing the geometry for the high-spin state. Once the minima are located and characterized (all frequencies are positive), consecutive restricted optimizations of the high-spin state, keeping fixed the collective angle θ (defined in section

3) but allowing a relaxation of the rest of the parameters, are performed till the crossing region is located. Thus, at each of the local restricted minima found, single point calculations for the BS solution are carried out. The energy difference between the quartet and the BS doublet at each geometry yields the coupling constant.

Theoretical Extraction of Magnetic Coupling Constant

The Hamiltonian describing the low-lying magnetic states of the system is the Heisenberg (more properly Heisenberg-Dirac-Van Vleck or HDVV) Hamiltonian,[11–14] with one $S = 1/2$ spin moment per each carbon sp^2 centre. It is defined as:

$$\hat{\mathcal{H}}^{\mathrm{HDVV}} = \sum_{<i,j>} J_{ij}\mathbf{S}_i \cdot \mathbf{S}_j = J_{12}\mathbf{S}_1 \cdot \mathbf{S}_2 + J_{23}\mathbf{S}_2 \cdot \mathbf{S}_3 + J_{13}\mathbf{S}_1 \cdot \mathbf{S}_3, \tag{1}$$

In the most general case, this spectrum involves the D_1, D_2 and Q states, which are pure spin states, meaning that they are eigenfunctions of the square of the total spin operator and of its z-component. These states can be expressed as a linear combination of the $|\alpha\alpha\beta\rangle$, $|\alpha\beta\alpha\rangle$ and $|\beta\alpha\alpha\rangle$ basis set elements which are eigenfunctions of the z-component of the total spin; the $+1/2$ component is chosen for convenience. By diagonalizing the matrix representation of the HDVV Hamiltonian in the above mentioned basis set, one obtains:[15]

$$|D_1\rangle = \frac{1}{\sqrt{2}}(|\alpha\alpha\beta\rangle - |\alpha\beta\alpha\rangle) \tag{2}$$

$$|D_2\rangle = \frac{1}{\sqrt{6}}(|\alpha\alpha\beta\rangle + |\alpha\beta\alpha\rangle - 2\,|\beta\alpha\alpha\rangle) \tag{3}$$

$$|Q\rangle = \frac{1}{\sqrt{3}}(|\alpha\alpha\beta\rangle + |\alpha\beta\alpha\rangle + |\beta\alpha\alpha\rangle) \tag{4}$$

and the corresponding eigenvalues are:

$$E_{D_1} = -1/4 \cdot (J_{12} + J_{13} + J_{23}) + 1/2 \cdot X \tag{5}$$

$$E_{D_2} = -1/4 \cdot (J_{12} + J_{13} + J_{23}) - 1/2 \cdot X \tag{6}$$

$$E_Q = -1/4 \cdot (J_{12} + J_{13} + J_{23}) \tag{7}$$

with

$$X = \sqrt{J_{12}^2 + J_{13}^2 + J_{23}^2 - J_{12} \cdot J_{13} - J_{12} \cdot J_{23} - J_{13} \cdot J_{23}} \tag{8}$$

from which the following expressions for the energy differences are obtained:

$$E_Q - E_{D_1} = 1/2(J_{12} + J_{13} + J_{23} - X) \tag{9}$$

$$E_Q - E_{D_2} = 1/2(J_{12} + J_{13} + J_{23} + X) \tag{10}$$

Now, the structural characteristics of the triradical studied permit a simplification of this spectrum, since the problem can be assumed to have the symmetry of an equilateral triangle. Thus, J_{12}, J_{23} and J_{13} are equal, the X term vanishes, the two doublet states D_1 and D_2 become degenerate and the relative position of the magnetic states is

$$E_Q - E_D = 3/2J \tag{11}$$

However, we are making use of the broken symmetry approach and therefore the functions that we are using to describe the doublet state are not eigenfunctions of the squared total spin operator, but functions that serve as basis set for the construction of the HDVV Hamiltonian, $|\alpha\alpha\beta\rangle$, $|\alpha\beta\alpha\rangle$ and $|\beta\alpha\alpha\rangle$. This procedure fits with the Ising Hamiltonian,[16] and actually the diagonal elements of both matrices (HDVV and Ising) are the same. It is defined as:

$$\hat{\mathcal{H}}^{\text{Ising}} = \sum_{<i,j>} J_{ij} S_i^z \cdot S_j^z = J_{12} S_1^z \cdot S_2^z + J_{23} S_2^z \cdot S_3^z + J_{13} S_1^z \cdot S_3^z, \tag{12}$$

The difference is that HDVV has non-diagonal elements different from zero, while Ising does not. The advantage of the Ising picture is that we can directly access the diagonal elements

of the matrix variationally minimizing the energy of the $|\alpha\alpha\beta\rangle$,$|\alpha\beta\alpha\rangle$ and $|\beta\alpha\alpha\rangle$ solutions, which is precisely what is done with density functional theory (DFT). Then, assuming the same equilateral triangle, the expressions for the energy of the quartet and broken symmetry doublet are:

$$E^{\text{Ising}}(|\alpha\alpha\alpha\rangle) = 3/4J \tag{13}$$

$$E^{\text{Ising}}(|\alpha\alpha\beta\rangle) = E^{\text{Ising}}(|\alpha\beta\alpha\rangle) = E^{\text{Ising}}(|\beta\alpha\alpha\rangle) = -1/4J \tag{14}$$

which implies:

$$E^{\text{Ising}}(|\alpha\alpha\alpha\rangle) - E^{\text{Ising}}(|\alpha\alpha\beta\rangle) = J \tag{15}$$

That is the expression that has been used in this work to extract the coupling constant from BS solutions.

Potential Energy Surface Investigated: Definition of the Angle

The reversal of the exchange coupling constant has been theoretically modelled following the torsion of the molecule along the collective angle θ, as defined in Fig.S4. The reported values in the main text refer to the angle defined as $\theta = (\theta_1 + \theta_2 + \theta_3 + \theta_4 + \theta_5 + \theta_6)/6$ where $\theta_1 - \theta_6$ are equal. The exact same profile is obtained when the restriction is less severe and the angle is defined as $\theta = (\theta_1 + \theta_3 + \theta_5)/3$.

4. ESR spectra of the triradical molecules

Rigid media ESR spectra of quartet molecules, like the studied triradical, consist on five signals whose separations depend on the zero-field splitting parameters, D and E, and whose distinct intensities are due to the different orientations of molecules with respect the external magnetic field, H. Thus, the weakest lines bounding the spectrum are produced by molecules whose z axes are parallel to the H direction whereas the signals of medium intensity are originated by molecules whose z axes are perpendicular to H while the most intense central line is generated by all molecules regardless their orientations.[17,18] The ESR spectra of the

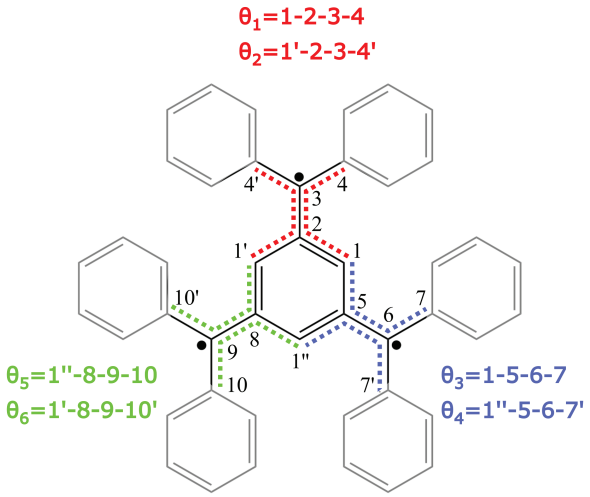

Figure S4: Schematic representation of the different angles used to performed the restricted optimizations.

studied triradical in frozen solutions of a 4:1 mixture of toluene and $CHCl_3$ at 145 K, where randomly oriented fixed molecules are present, exhibit the above described five signals[1] although the intensity of the central line is larger than that of a theoretically simulated spectrum (see Figure S5). This fact suggested that the observed central signal is composed by two overlapped lines: one corresponding to the central line of molecules with a quartet ground state, *i.e.* $J < 0$, and another due to molecules with a doublet ground state, *i.e.* $J > 0$. Both kinds of molecules were formed during the freezing process of the solution where the molecules get trapped in different conformations with distinct exchange couplings far from the thermodynamically most stable. In support of this affirmation is the fact that the ratio of double integrated signal intensities between the central and outer signals depends on the temperature ramp with which the solution was frozen (see Figures S6 and S7). Indeed, a slow temperature ramp leads to a ratio of 130 while a very rapid one gives a ratio of 180 which are very different from that theoretically expected. Another interesting observation is the fact that depending on the freezing conditions and nature of the solvent unfolded signals corresponding to quartet species were observed (Figure S8) indicating the presence of more than one quartet with different conformations.

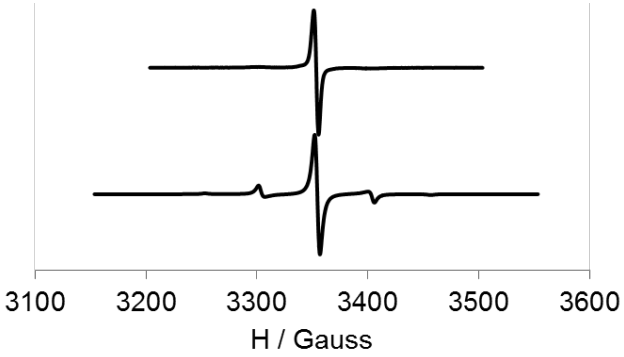

Figure S5: *Top*: Experimental spectrum of triradical at 145 K in toluene/$CHCl_3$ (4:1). *Bottom*: Simulated spectrum of a quartet with the central line having the same intensity than the experimental one. The ratio of double integrated areas between the central signal and the four outer signals in the simulated spectrum is c.a. 11.

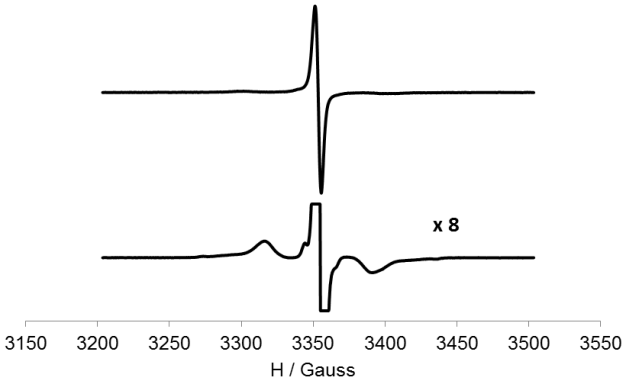

Figure S6: *Top*: Experimental spectra of triradical at 145 K in in toluene/$CHCl_3$ (4:1) obtained with a slow freezing temperature ramp. *Bottom*: Experimental spectrum magnified 8 times. The ratio of double integrated areas between the central signal and the four outer signals is c.a. 130.

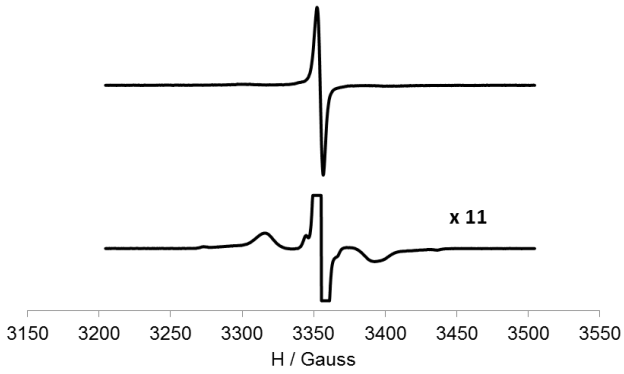

Figure S7: *Top*: Experimental spectra of triradical at 145 K in in toluene/$CHCl_3$ (4:1) obtained with a fast freezing temperature ramp. *Bottom*: Experimental spectrum magnified 11 times. The ratio of double integrated areas between the central signal and the four outer signals is c.a. 180.

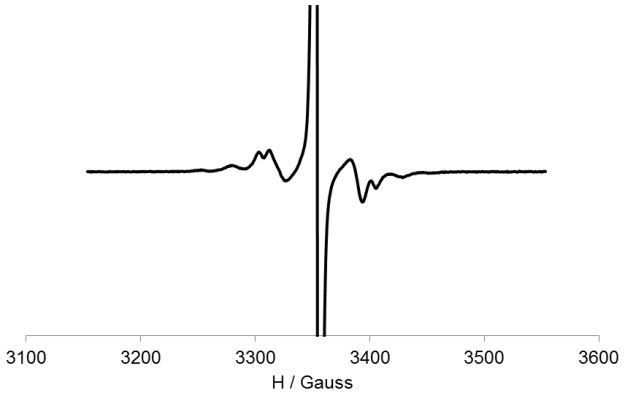

Figure S8: Experimental spectrum of triradical at 175 K in in toluene/$CHCl_3$ (4:1) obtained with a slow freezing temperature ramp using the same solution than in Figs. S6 and S7.

References

(1) Veciana, J.; Rovira, C.; Ventosa, N.; Crespo, M. I.; Palacio, F. *J. Am. Chem. Soc.* **1993**, *115*, 57–64.

(2) Burzurí, E.; Gaudenzi, R.; van der Zant, H. S. J. *J. Phys. Condens. Matter* **2015**, *27*, 113202.

(3) Frisch, M. J. et al. Gaussian 09, Revision A.1. 2009.

(4) Becke, A. D. *J. Chem. Phys.* **1993**, *98*, 5648.

(5) Hariharan, P. C.; Pople, J. A. *Theor. Chim. Acta* **1973**, *28*, 213–222.

(6) Francl, M. M. *J. Chem. Phys.* **1982**, *77*, 3654.

(7) Noodleman, L. *J. Chem. Phys.* **1981**, *74*, 5737.

(8) Noodleman, L.; Davidson, E. R. *Chem. Phys.* **1986**, *109*, 131–143.

(9) Noodleman, L.; Peng, C.; Case, D.; Mouesca, J.-M. *Coord. Chem. Rev.* **1995**, *144*, 199–244.

(10) Moreira, I. d. P. R.; Illas, F. *Phys. Chem. Chem. Phys.* **2006**, *8*, 1645–59.

(11) Heisenberg, W. *Zeitschrift fr Phys.* **1928**, *49*, 619–636.

(12) Dirac, P. A. M. *Proc. R. Soc. A Math. Phys. Eng. Sci.* **1929**, *123*, 714–733.

(13) Van Vleck, J. H. *The theory of electric and magnetic susceptibilities*; Oxford University Press: Oxford, 1932.

(14) Dirac, P. A. M. *Principles of Quantum Mechanics*; Clarendon Press: Oxford, 1958.

(15) Sinn, E. *Coord. Chem. Rev.* **1970**, *5*, 313–347.

(16) Ising, E. *Zeitschrift für Phys.* **1925**, *31*, 253–258.

(17) Kothe, G.; Ohmes, E.; Brickmann, J.; Zimmermann, H. *Angew. Chemie Int. Ed. English* **1971**, *10*, 938–940.

(18) Brickmann, J. *J. Chem. Phys.* **1973**, *59*, 2807.